JLR RESEARCH ARTICLE

Sialidase NEU3 action on GM1 ganglioside is neuroprotective in GM1 gangliosidosis

Maria L. Allende[1], Y. Terry Lee[1], Colleen Byrnes[1], Cuiling Li[1], Galina Tuymetova[1], Jenna Y. Bakir[1], Elena-Raluca Nicoli[2], Virginia K. James[3], Jennifer S. Brodbelt[3], Cynthia J. Tifft[2]*, and Richard L. Proia[1]*

[1]Genetics of Development and Disease Section, Genetics and Biochemistry Branch, National Institute of Diabetes and Digestive and Kidney Diseases, and [2]Medical Genetics Branch, National Human Genome Research Institute, National Institutes of Health, Bethesda, MD, USA; [3]Department of Chemistry, University of Texas at Austin, Austin, TX, USA

Abstract GM1 gangliosidosis is a neurodegenerative disorder caused by mutations in the *GLB1* gene, which encodes lysosomal β-galactosidase. The enzyme deficiency blocks GM1 ganglioside catabolism, leading to accumulation of GM1 ganglioside and asialo-GM1 ganglioside (GA1 glycolipid) in brain. This disease can present in varying degrees of severity, with the level of residual β-galactosidase activity primarily determining the clinical course. *Glb1* null mouse models, which completely lack β-galactosidase expression, exhibit a less severe form of the disease than expected from the comparable deficiency in humans, suggesting a potential species difference in the GM1 ganglioside degradation pathway. We hypothesized this difference may involve the sialidase NEU3, which acts on GM1 ganglioside to produce GA1 glycolipid. To test this hypothesis, we generated *Glb1/Neu3* double KO (DKO) mice. These mice had a significantly shorter lifespan, increased neurodegeneration, and more severe ataxia than *Glb1* KO mice. *Glb1/Neu3* DKO mouse brains exhibited an increased GM1 ganglioside to GA1 glycolipid ratio compared with *Glb1* KO mice, indicating that NEU3 mediated GM1 ganglioside to GA1 glycolipid conversion in *Glb1* KO mice. The expression of genes associated with neuroinflammation and glial responses were enhanced in *Glb1/Neu3* DKO mice compared with *Glb1* KO mice. Mouse NEU3 more efficiently converted GM1 ganglioside to GA1 glycolipid than human NEU3 did. Our findings highlight NEU3's role in ameliorating the consequences of *Glb1* deletion in mice, provide insights into NEU3's differential effects between mice and humans in GM1 gangliosidosis, and offer a potential therapeutic approach for reducing toxic GM1 ganglioside accumulation in GM1 gangliosidosis patients.

Supplementary key words brain lipids • glycolipids • inflammation storage diseases • sphingolipids

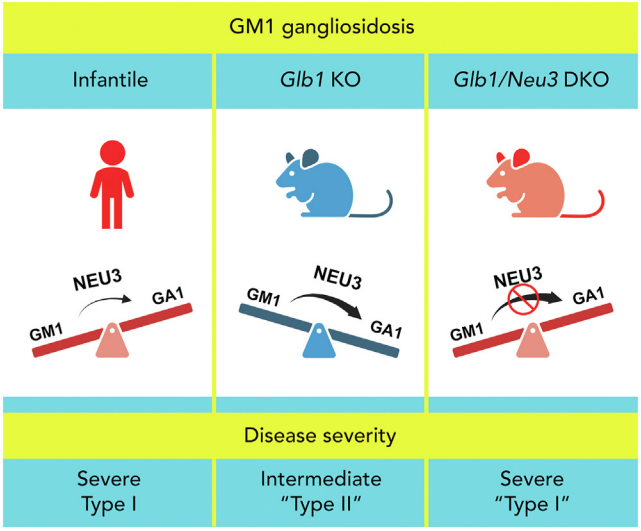

GM1 gangliosidosis is a rare lysosomal storage disorder that affects the central nervous system, resulting in the accumulation of GM1 ganglioside and asialo-GM1 ganglioside (GA1 glycolipid) in the brain (1, 2). The disease is caused by mutations in the *GLB1* gene, which encodes for acid β-galactosidase, an enzyme responsible for removing the terminal β-linked galactose from glycolipids and other substrates. The age of onset and severity of symptoms in GM1 gangliosidosis patients depend on the amount of residual β-galactosidase activity permitted by each patient's particular *GLB1* gene mutation(s).

Infantile GM1 gangliosidosis, known as type I, is the most severe form of the disease, characterized by little or nondetectable β-galactosidase activity. Infants with this form of the disease show rapid and progressive neurodegeneration, leading to death within the first few years of life. Juvenile and adult presentations, known as type II and type III, respectively, are milder forms of the disease, due to the presence of some

*For correspondence: Richard L. Proia, proia@nih.gov; Cynthia J. Tifft, cynthiat@mail.nih.gov.

https://doi.org/10.1016/j.jlr.2023.100463

residual β-galactosidase enzymatic activity. These forms are characterized by slower disease progression and longer survival times. Interestingly, *Glb1* null mouse models, which totally lack lysosomal β-galactosidase activity, exhibit a less severe form of the disease than expected based on comparable enzyme deficiencies in humans (3), suggesting the existence of a disease-modifying GM1 ganglioside degradation pathway in mice.

In this study, our objective was to investigate the underlying reason for the discrepancy in disease severity between humans and mice with null *GLB1*/*Glb1* genes. Our findings suggest that enhanced activity of the sialidase NEU3 (4–7) in the mouse ganglioside catabolism pathway, as compared with the human system, contributes to this difference. Consequently, our results identify the sialidase NEU3 as a potential therapeutic target for reducing toxic GM1 ganglioside accumulation in individuals with GM1 gangliosidosis.

MATERIALS AND METHODS

Mouse generation and characterization

Glb1 KO mice were generated using CRISPR/Cas9 as described (3). The mutant mice carry a 17 bp deletion in exon 2 and a 28 bp deletion in exon 6. The deletion in exon 2 results in a frameshift and predicted premature termination within exon 3 (3).

Glb1 KO mice were genotyped by PCR of tail-snip DNA using the following primers and PCR conditions:

Glb1_ex6_For 5′- CTGCTGATCTCTGGTCCTCCTT -3′

Glb1_ex6_Rev 5′- TCTAGATGCTACCTACACACACC -3′

PCR conditions were as follows: denaturation, 94°C for 10 min; amplification, 94°C for 15 s, 62°C for 10 s, 72°C for 20 s; and extension, 72°C for 7 min (40 cycles). The expected product size for the *Glb1*_WT allele is 242 bp and for the *Glb1*_targeted allele is 214 bp.

To generate *Neu3* KO mice, four single guide RNAs (Synthego, Redwood City, CA) corresponding to sequences on exon 2 (ACCGGATCCCAGCCCTGCTG, GCGGACCTCAGTCAGAGATG) and on exon 3 (GAGAGGTGCCAGATTGTGTG, CTACTCAGAAGTGCCCTCTG) and Cas9 protein (Synthego) were microinjected into C57BL/6J mouse embryos. The injected embryos were implanted into pseudopregnant surrogate female mice (8). The offspring were screened by PCR to identify mice carrying insertions or deletions in exon 2/3. The following primers flanking exon 2 were used:

Neu3_Exon2_For 5′- CTAGAGAACAGAGTTGTTGCA TGAGG -3′

Neu3_Exon3_Rev2 5′- GGTTCCGGTTGTAGTAGATG CCTA -3′

A founder mouse carrying a 10,043 bp deletion that included exon 2 and a portion of exon 3 was identified (supplemental Fig. S1A). This founder mouse was backcrossed to C57BL/6J mice (The Jackson Laboratory, Bar Harbor, ME) to derive mouse colonies carrying the *Neu3* KO allele.

Neu3 KO mice were genotyped by PCR of tail-snip DNA using the following primers and PCR conditions:

Neu3_For1 5′- CTAGAGAACAGAGTTGTTGCAT GAGG -3′

Neu3_Rev13 5′- GAGGCCTGTAGCAGTGAATTAGT-TAAAC -3′

Neu3_Rev5 5′- GCTAGTTGGATGTGAGTACAAGAG -3′

PCR conditions were as follows: denaturation, 94°C for 10 min; amplification, 94°C for 30 s, 63°C for 30 s, 72°C for 1 min; and extension, 72°C for 7 min (40 cycles). The expected product size for the *Neu3*_WT allele is 502 bp and for the *Neu3*_targeted allele is 328 bp.

Ataxia was quantified to determine disease severity. Briefly, each animal was subjected weekly to a set of six assessments, adapted from (9), which were recorded on a scale of 0–3 (0 represented absence of the abnormal phenotype and 3 represented the most severe manifestation). The score was produced using the sum of the six assessment values for a single mouse. The measures used were as follows: the ledge test to measure coordination; hindlimb clasping; gait to test coordination and muscle function; kyphosis as a manifestation of neurodegeneration; stance; and hindlimb locomotion. In addition, mice were weighed weekly, starting at 4 weeks of age.

All animal procedures were approved by the National Institute of Diabetes and Digestive and Kidney Diseases Animal Care and Use Committee and were performed in accordance with National Institutes of Health guidelines.

GM1 gangliosidosis patient samples

The GM1 gangliosidosis tissue samples included in this study were from patients enrolled in National Institutes of Health protocol, "Natural History of Glycosphingolipid Storage Disorders and Glycoprotein Disorders" (IRB# 09-HG-0107, NCT00029965), approved by the National Human Genome Research Institute Institutional Review Board. Patient samples were acquired with parental consent. All studies involving human subjects abide by the Declaration of Helsinki principles.

Glycosphingolipid extraction and analysis

Total lipids were isolated from mouse brain (one hemisphere) and from a portion of cerebral cortex from male infantile GM1 gangliosidosis patient using three sequential extractions: 10 volumes (vol) (v/weight) each of chloroform:methanol (C:M) (1:1 v/v), then 10 vol of C:M (1:2 v/v), and finally 10 vol of C:M:water (W) (30:60:8 v/v/v), each time for 16 h at room temperature. The combined lipid extracts were dried under nitrogen, dissolved in 9 ml C:M (2:1 v/v), and partitioned into two phases after the addition of 0.2 vol of 0.1 M KCl (10).

Gangliosides were enriched from the upper (aqueous) phase as follows. The upper phase was desalinated using a Sep-Pak C18 column (part # WAT020805; Waters, Milford, MA), previously washed with 3 column vol of methanol, 5 column vol of M:W (1:1 v/v), and 2 column vol of 0.1 M KCl. After sample application, columns were washed with 5 column vol of water and gangliosides eluted by adding 2 ml of methanol followed by 6 ml of C:M (1:1 v/v). The eluate was dried and then dissolved in 200 μl of C:M:W (30:60:8 v/v/v). A 10 μl aliquot was applied to high-performance TLC (HPTLC) plates (catalog # 1.05641.0001, Supelco, Sigma-Aldrich, Burlington, MA) and developed in C:M:0.2% $CaCl_2$ (55:45:10 v/v/v) or in C:M:0.25% $CaCl_2$ (60:35:8 v/v/v). Gangliosides were detected on the plates using resorcinol-HCl spray (11) as blue-violet bands. Individual gangliosides were identified by comparison with bovine brain ganglioside standards (catalog # 1065; Matreya LLC, State College, PA)

and monosialogangliosides standards (catalog # 1508; Matreya LLC) applied on the same HPTLC plate.

Glycosphingolipids were enriched from the lower (organic) phase as follows. After mild alkaline treatment in 0.1 N NaOH at 40°C for 2 h, extracts were neutralized with 2 M acetic acid, then partitioned into two phases after the addition of 0.2 vol of 0.1 M KCl. The second lower phases were dried under nitrogen, resuspended in 3 ml of methanol, and partitioned with 5 ml of n-hexane. The lower methanol-rich phase was separated, dried under nitrogen, and resuspended in 200 µl of C:M (1:1 v/v).

To determine amounts of GM1 ganglioside and GA1 glycolipid in brain, a 10 µl aliquot of upper organic phase plus a 10 µl aliquot of lower aqueous phase corresponding to the same brain tissue sample were applied to the same lane on an HPTLC plate. The plate was run in C:M:0.25% $CaCl_2$ (60:35:5 v/v/v), treated with orcinol spray (12), and imaged on the Amersham Imager 680 (Cytiva, Marlborough, MA) for quantification using ImageQuant TL software (Cytiva). Absolute amounts of GM1 ganglioside and GA1 glycolipid in mouse brain were determined based on a standard curve generated with known quantities of GM1 ganglioside (monosialogangliosides standards, catalogue # 1508; Matreya LLC) and GA1 glycolipid (catalogue #3018, Sigma-Aldrich).

LC-MS/MS of gangliosides

Dried ganglioside extracts were reconstituted in DMSO to ~3 µg/µl, which were further diluted to ~30 ng/µl in LC starting conditions (15% mobile phase B). A Dionex Ultimate 3000 UHPLC system (Thermo Fisher Scientific, Waltham, MA) was coupled to a Orbitrap Fusion Lumos mass spectrometer (Thermo Fisher Scientific) modified to perform ultraviolet photodissociation (UVPD) via a 193 nm Coherent ExciStar XS excimer laser (Santa Clara, CA), as previously described (13). An Agilent Poroshell 120 EC-C18 column (3 mm × 150 mm, 2.7 µm particles) (Agilent, Santa Clara, CA) was used for chromatographic separations with mobile phases (A) 60:40 acetonitrile/W (v/v) and (B) 90:10 v/v isopropanol/acetonitrile, both with 0.1% formic acid and 10 mM ammonium formate. A flow rate of 250 µl/min was used with a linear gradient of 15%–90% mobile phase B over 20 min, followed by a flush for 3 min with 90% mobile phase B, and then re-equilibrated for 5 min with 15% mobile phase B before injection of the next sample. The column temperature was 40°C, and ~300 ng of each sample was injected. A data-dependent method was implemented with UVPD (7 pulses, 2.5 mJ per pulse) to generate MS2 UVPD spectra of the top eight most abundant precursor ions in the MS1 spectra. This UVPD data was only used for identification of gangliosides, not quantitation. A resolution of 30,000 (m/z 200) and two µscans were used for acquisition of both MS1 and UVPD spectra. Three technical replicates were collected with only MS1 spectra for the quantitation of gangliosides in each of the three biological replicates for each sample group.

UVPD fragmentation was used to manually identify all gangliosides by comparing fragments to theoretical fragments derived by the LIPID Metabolites and Pathways Strategy structure database (www.lipidmaps.org). As described in a prior report, UVPD provides detailed fragmentation patterns of gangliosides, including fragment ions that originate from cleavages of acyl chain bonds that enable the elucidation of acyl chain length (14). Extracted ion chromatograms were generated in Qual Browser (Thermo Fisher Scientific) for each ganglioside in each technical replicate, and each peak area was calculated using the Genesis algorithm in Qual Browser. Peak areas were summed for all gangliosides in each replicate, and the peak area for each individual ganglioside was reported as the percentage of total ganglioside peak area. Peak area for each biological replicate was determined from the average of three technical replicates per sample. There were three biological replicates per sample group, and their average peak area and SDs are reported in supplemental Fig. S1C.

Western blotting

Fibroblast and brain extracts were prepared in RIPA lysis and extraction buffer (Thermo Fisher Scientific) supplemented with HALT protease inhibitor cocktail (Thermo Fisher Scientific) and HALT phosphatase inhibitor cocktail (Thermo Fisher Scientific). Samples were incubated 30 min on ice and later spun at 13,000 RPM at 4°C for 15 min. Samples (30 µg) were resolved on a 4%–12% Bis-Tris gel (Thermo Fisher Scientific) together with a molecular weight protein standard (LC5800, Thermo Fisher Scientific), then transferred to nitrocellulose membranes using the iBlot2 Blotting System (Thermo Fisher Scientific). The membranes were blocked in 5% nonfat dry milk, 0.05% Tween 20 in TBS, then probed with antibodies against Strep-Tag II to detect NEU3 fusion proteins (catalog # MA5-37747; Thermo Fisher Scientific) or p62/SQSTM1 (catalog # P0067; Sigma-Aldrich). Primary antibodies were detected by incubation with a secondary goat anti-rabbit IgG, peroxidase-conjugated antibody (catalog # AP132P; Sigma-Aldrich). Membranes were reprobed with anti-mouse β-actin (monoclonal AC-15, HRP-conjugated, catalog # ab49900) from Abcam (Cambridge, MA) to provide a loading control. Membranes were developed using the chemiluminescence reagents (ECL Prime Western blotting System, catalog # GERPN2232; Sigma-Aldrich), signals visualized using the Amersham Imager 680 imager and quantified using ImageQuant TL software.

RNA-seq analysis

Brains (n = 5) from WT, *Glb1* KO, *Neu3* KO, and *Glb1/Neu3* DKO mice were harvested at 20 weeks of age. RNA-seq analysis was performed as described (15). Briefly, total RNA from one brain hemisphere was isolated using the miRNeasy Mini Kit from Qiagen (catalog # 217004; Redwood City, CA). Preparation of the RNA library, mRNA sequencing, and bioinformatic analysis was performed by Novogene (Beijing, China). Libraries were sequenced on an Illumina PE150 platform (Illumina, San Diego, CA) for 40 million paired-end reads for each sample. All high-quality clean reads were mapped to reference genome mm10 (GRCm38) using hisat2 (version 2.0.5). Gene expression quantification was performed using featureCounts (version 1.5.0-p3) and differential analysis performed using DESeq2 (version 1.20.0). Genes were considered differentially expressed when the expression levels between samples showed a 2-fold change (log_2(-fold-change) >+1 or <−1) with adjusted $P < 0.05$. Pathway enrichment Gene Ontology analysis was performed using clusterProfiler (version 3.8.1) with corrected P-value set to <0.05 for significant enrichment.

Brain silver staining

NeuroSilver staining was performed by FD NeuroTechnologies (Columbia, MD) using the FD NeuroSilver kit II

to detect degenerating neurons. Sagittal brain sections were cut at 40 μm, stained, and then imaged under a Keyence microscope (Model BZ-X800; Keyence, Itasca, IL). To quantify the silver staining of the brains, three Z-stacks (22–37 images per stack) were captured from brain stem, thalamus, and cortex from three mice per genotype under a 40×-oil objective using the same microscope settings. The silver-stained area for each stack was quantified by thresholding using Fiji/ImageJ (16).

BODIPY-GM1 ganglioside degradation in human fibroblasts

Human fibroblasts from an infantile GM1 gangliosidosis patient carrying two heterozygous *GLB1* mutations, c.176G>A (Arg59His) and c.765G>C (Gln255His), were generated from a skin biopsy. Fibroblast were grown in DMEM Glutamax (catalog #10569044, Thermo Fisher Scientific) supplemented with 10% fetal bovine serum and 100 U/ml penicillin-streptomycin (catalog #10140148, Thermo Fisher Scientific). Viral transduction was performed by plating 100,000 cells in a 24-well tissue culture plate until they achieved 50%–70% confluency, then cells were incubated with lentiviral particles (VectorBuilder, Chicago, IL) carrying mouse *Neu3*, human *NEU3*, or a control vector (supplemental Fig. S2) at a multiplicity of infection of 10. Puromycin (Thermo Fisher Scientific) was added 48 h posttransduction at 1 μg/ml to obtain stable expression after 7 days.

Transduced fibroblasts were seeded into 6-well plates (3×10^5 cells per well) and, after 72 h, incubated with 2 μM BODIPY-GM1 ganglioside (catalog # 33799, Cayman, Ann Arbor, MI) in DMEM, 10% FBS for 72 h at 37°C. Fibroblasts were then harvested, and lipids were extracted with C:M (2:1 v/v) overnight at room temperature. Total lipid extracts were separated by HPTLC using C:M:0.25% $CaCl_2$ (60:35:5 v/v/v). BODIPY-labeled GM1 ganglioside and GA1 glycolipid were identified using BODIPY-labeled standards run on the same plate. Labeled bands were visualized using the Amersham Imager 680 imager and quantified using ImageQuant TL software. BODIPY-GA1 glycolipid standard was generated after hydrolysis of BODIPY-GM1 ganglioside (Cayman) with *Clostridium perfingens* neuraminidase (catalog # 11 585 886 001, Sigma-Aldrich, St. Louis, MO) as previously described (17).

Real-time quantitative PCR

Total RNA was isolated from WT, *Neu3* KO, and *Glb1* KO mouse brain using miRNeasy Mini Kit (catalog #217004, Qiagen, Redwood City, CA) following manufacture's protocol. Two micrograms of total RNA were reversed transcribed into cDNA using SuperScript IV VILO Master Mix (catalogue #11756050, Thermo Fisher Scientific) following manufacture's protocol. The real-time quantitative PCR was conducted with 5 ng of cDNA from each genotype using Quant Studio 7 with TaqMan Gene Expression Master Mix (catalog #4369016, Thermo Fisher Scientific). TaqMan probe for mouse *Neu3* (mouse *Neu3*: Mn00479379_m1) and β actin (*Actb*: Mn00607939S1) were purchased from Thermo Fisher Scientific. Relative gene expression analysis was performed with β actin as endogenous control.

Statistical analyses

Comparisons were analyzed for statistical significance using unpaired *t* test or one-way Anova with Bonferroni correction. All results were presented as means ± SD, and a value for $P < 0.05$ was considered statistically significant.

RESULTS

Neu3 disruption increases disease severity in *Glb1* KO mice

Genetic disruption of the gene encoding for lysosomal β-galactosidase, *Glb1*, in mice causes GM1 ganglioside and GA1 glycolipid accumulation in the brain, progressive neurodegeneration, and a shortened lifespan (18–22). However, *Glb1* KO mice resemble the less severe type II form of the disease in humans, instead of the most severe type I infantile form as would be expected from the null *Glb1* mutations (3). This outcome suggested that a disease-modifying pathway that mitigates the consequences of *Glb1* deletion may exist in mice. Previous studies have described a mouse-specific alternative catabolic pathway, involving the sialidase NEU3 for the degradation of GM2 ganglioside (**Fig. 1**A) that is less active in humans (6). To investigate whether NEU3 also contributes to GM1 degradation and symptom amelioration in GM1 gangliosidosis mice, we first generated a *Neu3* KO mouse line by CRISPR/Cas9 gene disruption (8) that carried an approximately 10 kb deletion, which included the entire *Neu3* exon 2 and the coding region in exon 3 (supplemental Fig. S1A). No *Neu3* mRNA expression was detected in the brains of *Neu3* KO mice, confirming a null allele (supplemental Fig. S1B). LC-MS/MS profiling revealed that WT and *Neu3* KO brain lipid extracts displayed a similar spectrum of ganglioside species (supplemental Fig. S1C). *Neu3* KO mice appeared grossly normal as has been described for another independently derived *Neu3* KO mouse line (23).

The *Neu3* and *Glb1* KO mice were then bred to produce *Glb1/Neu3* DKO mice. The *Glb1/Neu3* DKO mice began losing weight after about 15 weeks and died between 20 and 24 weeks of age. This course was substantially earlier than what was observed for the *Glb1* KO mice, which started to lose weight after 30 weeks of age and died between 44 and 47 weeks of age (Fig. 1B–D). Compared with the *Glb1* KO mice, the *Glb1/Neu3* DKO mice displayed a significantly higher ataxia score between 14 and 22 weeks of age, consistent with a worsened neurodegenerative phenotype (Fig. 1E). The WT and *Neu3* KO mice did not show weight loss, premature demise, or signs of ataxia over time (Fig. 1B, C). Compared with the brains of WT or single KO mice, the brains of the *Glb1/Neu3* DKO mice contained significantly increased levels of p62 (supplemental Fig. S3), an indicator of impaired autophagy, as has been demonstrated in several lysosomal storage diseases with neurodegeneration (24). These results demonstrate a critical role of the sialidase NEU3 in extending the life span and ameliorating the neurodegenerative phenotype caused by the *Glb1* deletion in mice.

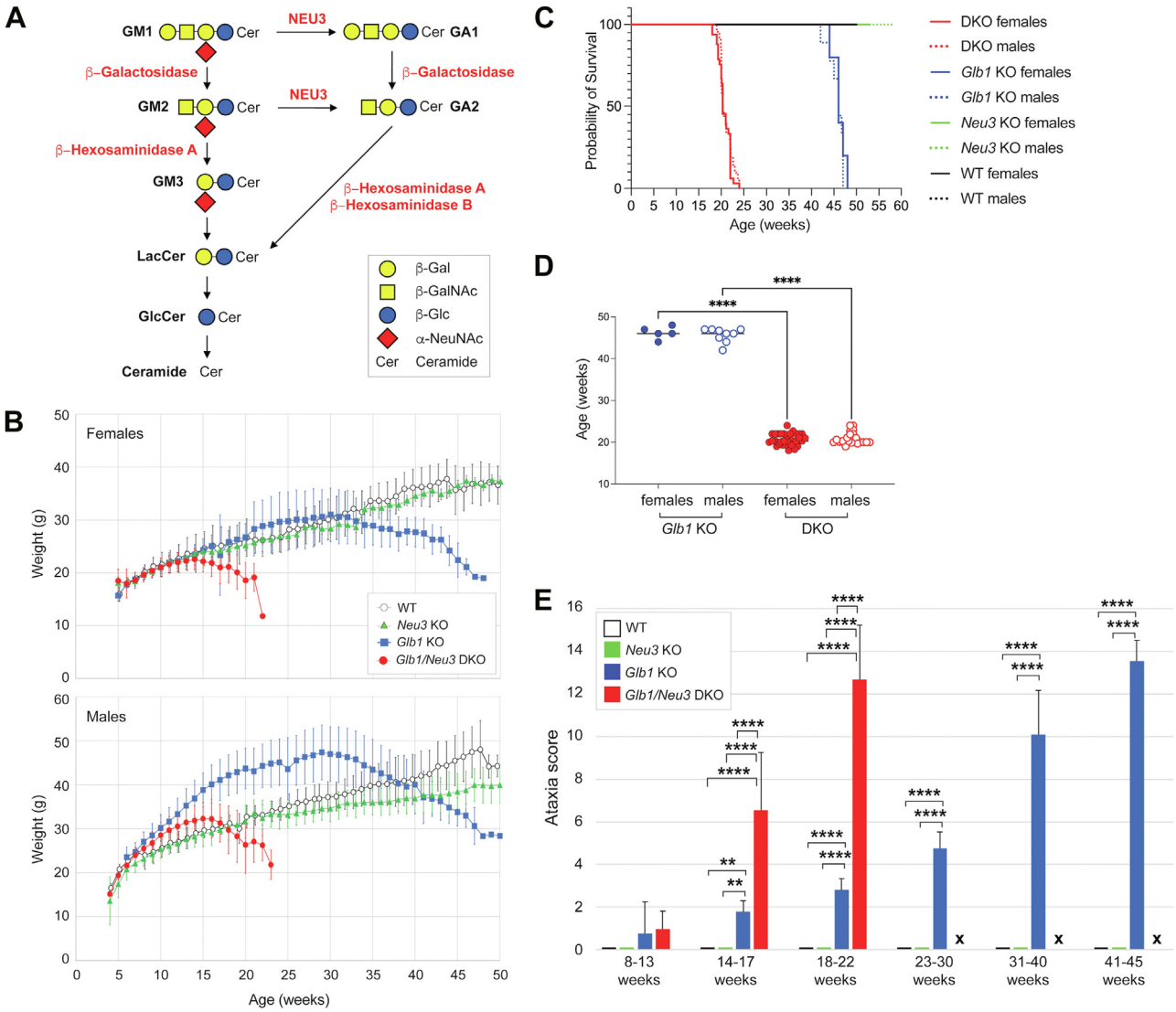

Fig. 1. *Neu3* disruption increases disease severity in *Glb1* KO mice. A: Schematic illustrating the degradation pathway of GM1 ganglioside. B, C: Kaplan–Meier survival plot (B) and mean survival (C) for female and male *Glb1* KO and *Glb1/Neu3* DKO mice. Data are expressed as percent survival at each time (B) and as mean lifespan (C). Statistical significance was determined by one-way ANOVA with Bonferroni correction, ****$P < 0.0001$. *Glb1* KO females, n = 5; *Glb1* KO males, n = 9; *Glb1/Neu3* DKO females, n = 33; *Glb1/Neu3* DKO males, n = 21. D: Body-weight progression determined weekly for WT, *Neu3* KO, *Glb1* KO, and *Glb1/Neu3* DKO mice. Top graph, female mice; bottom graph, male mice. Data are expressed as means ± SD for each timepoint. WT females and males, n = 11; *Neu3* KO females and males, n = 15; *Glb1* KO females, n = 11 and males, n = 14; *Glb1/Neu3* DKO females, n = 21 and males, n = 11. E: Quantification of disease severity through ataxia phenotype scoring. Mice were scored weekly based on six parameters for 45. Each measurement was recorded on a scale of 0 (no symptoms) to 3 (most severe), with a combined total ataxia score from 0 to 18. Scores for the time period shown on the graph were grouped and averaged. x, *Glb1/Neu3* DKO mice did not survive beyond 22 weeks of age. Data are expressed as means ± SD. Statistical significance was determined by one-way ANOVA with Bonferroni correction, **$P < 0.01$; ****$P < 0.0001$. WT: 8–13 weeks, n = 18; 14–17 weeks, n = 8; 18–22 weeks, n = 3, 23–30 weeks, n = 2; 31–40 weeks, n = 4, 41–45 weeks, n = 22. *Neu3* KO: 8–13 weeks, n = 2; 14–17 weeks, n = 4; 18–22 weeks, n = 4, 23–30 weeks, n = 4; 31–40 weeks, n = 5, 41–45 weeks, n = 6. *Glb1* KO: 8–13 weeks, n = 7; 14–17 weeks, n = 14; 18–22 weeks, n = 11, 23–30 weeks, n = 9; 31–40 weeks, n = 23, 41–45 weeks, n = 32. *Glb1/Neu3* DKO: 8–13 weeks, n = 33; 14–17 weeks, n = 30; 18–22 weeks, n = 16. Cer, ceramide; DKO, double KO; GlcCer, glucosylceramide; LacCer, lactosylceramide.

GM1 ganglioside to GA1 glycolipid conversion is blocked in *Glb1/Neu3* DKO mouse brain

We determined ganglioside and neutral glycosphingolipid levels in the brains of 20-week-old WT, *Glb1* KO, *Neu3* KO, and *Glb1/Neu3* DKO mice by HPTLC. The results showed that the ganglioside and neutral glycosphingolipid patterns in the *Neu3* KO brain were similar to those observed in the WT brain (Fig. 2A, B). However, both *Glb1* KO and *Glb1/Neu3* DKO brains from 20-week-old mice exhibited an accumulation of GM1 ganglioside and GA1 glycolipid (Fig. 2A, B). The *Glb1* KO brains had lower levels of GM1 ganglioside than the *Glb1/Neu3* DKO brains. On the other hand, the GA1 glycolipid levels in *Glb1* KO brains

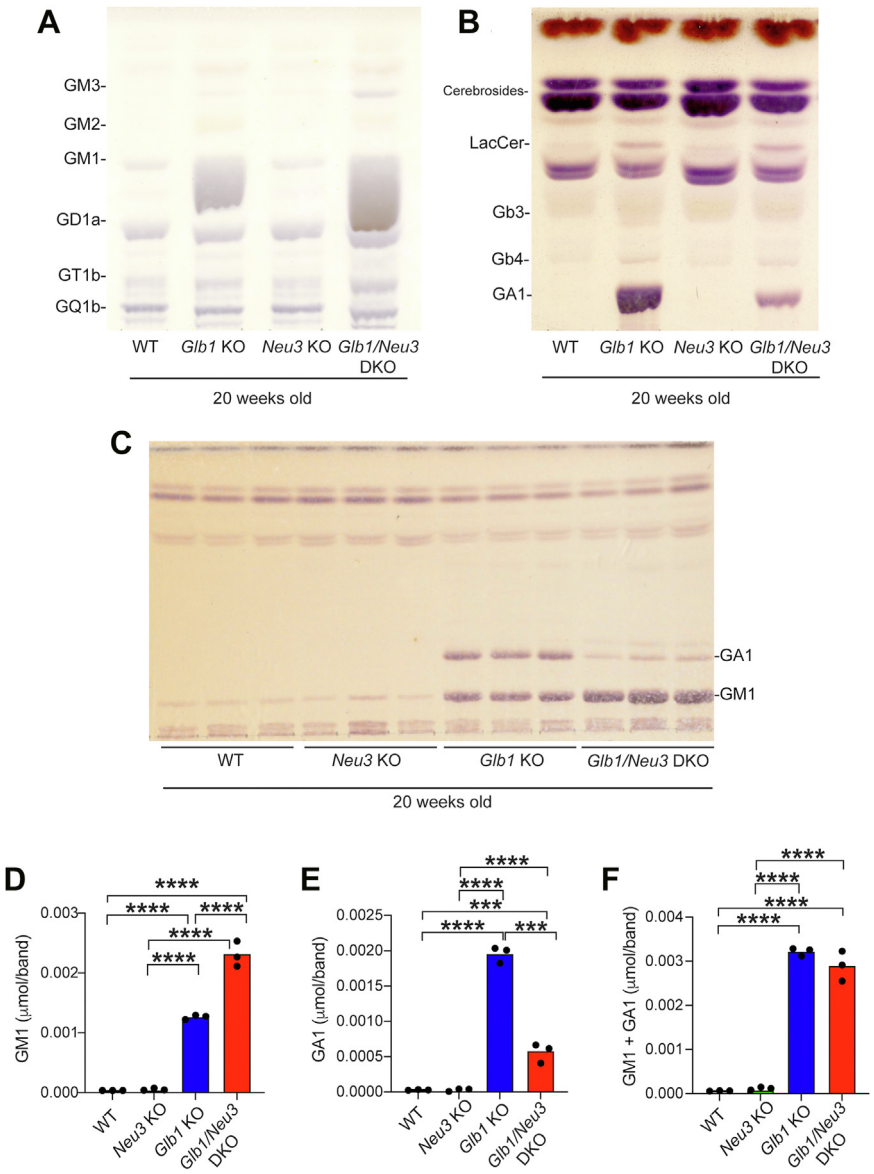

Fig. 2. GM1 ganglioside to GA1 glycolipid conversion is blocked in *Glb1/Neu3* DKO mouse brain. Brains from *Glb1/Neu3* DKO, *Glb1* KO, *Neu3* KO, and WT mice were harvested at 20 weeks of age (n = 3 each genotype) and fractions that contain gangliosides (aqueous) and other glycosphingolipids (organic) were analyzed. Representative images were included in A–C. A: Aqueous fraction; an equivalent of approximately 13 mg wet-brain weight was applied to an HPTLC plate, developed in C:M:0.2% $CaCl_2$ (55:45:10 v/v/v), and visualized using resorcinol. Major gangliosides were identified using standards run on the same HPTLC plate. B: Organic fraction; an equivalent of approximately 13 mg wet-brain weight was applied to an HPTLC plate, developed in C:M:W (60:25:4 v/v/v), and visualized using orcinol. Major neutral glycosphingolipids were identified using standards run on the same HPTLC plate. C: Aqueous and organic fractions equivalent to 0.65 mg wet-brain weight were applied to the same lane on an HPTLC plate, developed in C:M:0.25% $CaCl_2$ (60:35:5 v/v/v), and visualized using orcinol. GM1 ganglioside and GA1 glycolipid positions were identified using standards run on the same HPTLC plate. D–F: Quantification of band intensities from the HPTLC plate in (C). Standard curves of known amounts of GM1 ganglioside and GA1 glycolipid run on the same HPTLC plate were used to determine the total amounts of GM1 ganglioside and GA1 glycolipid for each mouse brain. Data are expressed as means (three mice per genotype). Statistical significance was determined by one-way ANOVA with Bonferroni correction, ***$P < 0.001$, ****$P < 0.0001$. n = 3 for each genotype. GA1, GM1 and asialo-GM1 ganglioside; HPTLC, high-performance TLC.

were higher than in *Glb1/Neu3* DKO brains (Fig. 2C–F). These findings suggest that the absence of the sialidase NEU3 in *Glb1/Neu3* DKO mice impedes the removal of sialic acid from GM1 ganglioside to form GA1 glycolipid. Importantly, the total combined level of GM1 ganglioside and glycolipid GA1 was not significantly different between *Glb1/Neu3* DKO and *Glb1* KO brains (Fig. 2F). This finding implies that once NEU3 converts GM1 ganglioside to glycolipid GA1 in the *Glb1* KO, any further degradation is blocked.

Neuroinflammatory and glial reaction gene expression is enhanced in *Glb1/Neu3* DKO mouse brain

We conducted RNA-seq analysis on the brains of 20-week-old *Glb1/Neu3* DKO, *Glb1* KO, *Neu3* KO, and WT

mice. The results revealed that the top Gene Ontology Biological Process categories, ranked by significance when comparing *Glb1/Neu3* DKO and WT mice, were primarily associated with immune and inflammatory responses (**Fig. 3**A). The heatmap analysis of genes within the positive regulation of cytokine production category across the four genotypes demonstrated a pattern of substantially higher expression in the DKO mice than *Glb1* KO, *Neu3* KO, and WT mice (Fig. 3B).

To visualize the expression of the 25 most significant differentially expressed genes between *Glb1/Neu3* DKO and WT brains (supplemental Table S1) across all genotypes, we generated a heatmap of gene expression to include the individual mice in each of the four

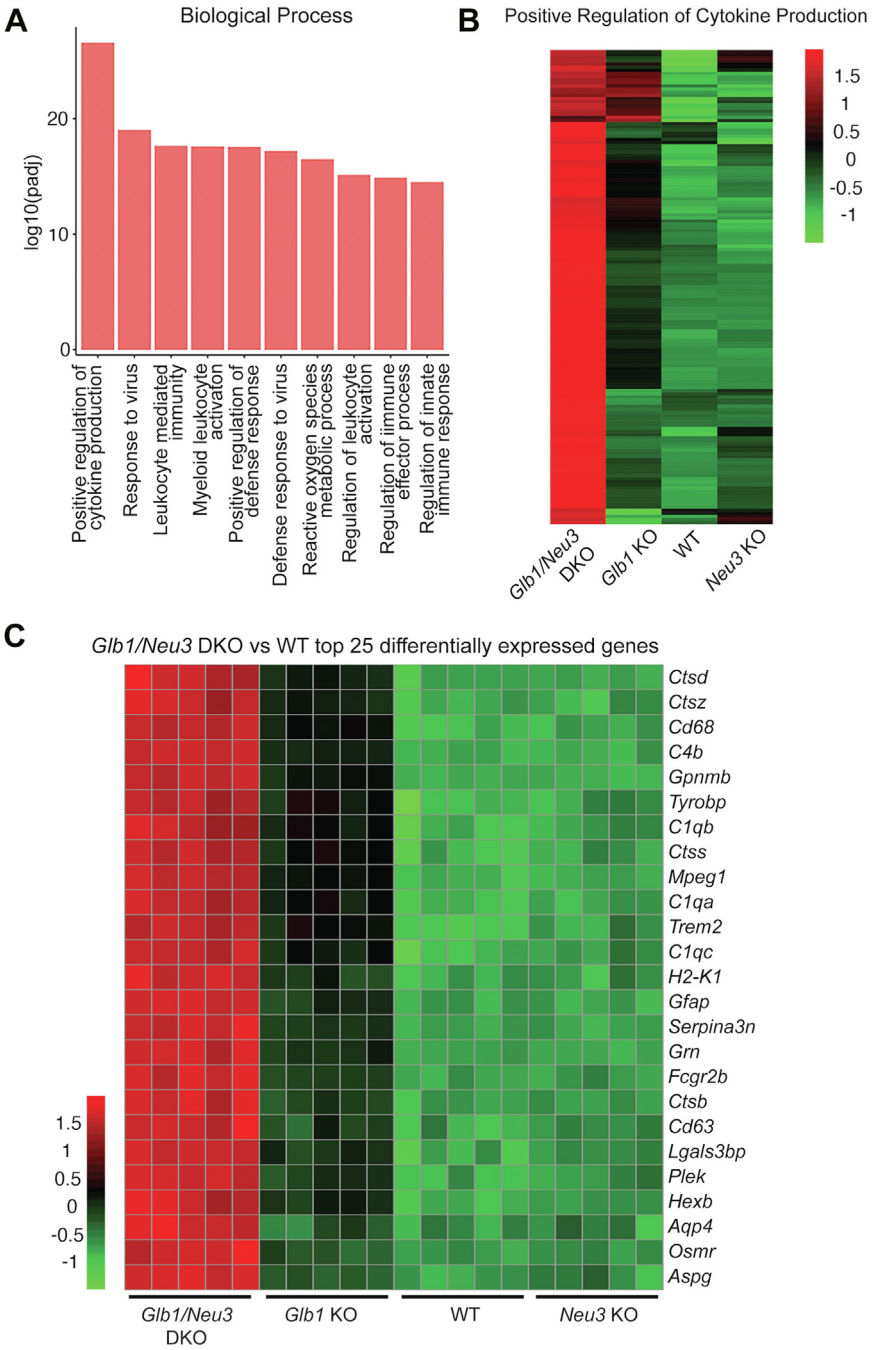

Fig. 3. Neuroinflammatory and glial reaction gene expression is enhanced in *Glb1/Neu3* DKO mouse brain. Brains from *Glb1/Neu3* DKO, *Glb1* KO, *Neu3* KO, and WT mice were harvested at 20 weeks of age (n = 5 each) and RNA isolated for RNA-seq analysis. A: Top 10 GO: Biological Process categories that are differentially regulated between WT and *Glb1/Neu3* DKO mice. B: Heatmap indicating the mean row Z-score of individual gene expression for each genotype in the GO: Positive Regulation of Cytokine Production category. C: Heatmap indicating the row Z-score of individual gene expression of the top 25 most significant differentially expressed genes between WT and *Glb1/Neu3* DKO mice for each genotype. Each vertical column represents an individual mouse. DKO, double KO; GO, Gene Ontology.

genotypes (Fig. 3C). The results indicated that the DKO brains displayed elevations in gene expression associated with astrocytes (*Gfap*, *Aqp4*, *Aspg*) and microglia/macrophages (*Cd68*, *Hexb*, *Mpeg1*, *Trem2*, *Tyrobp*, *Gpnmb*), indicating increased glial responses (25–27). Furthermore, genes associated with neuroinflammation (*C4b*, *C1qa/b/c*, *Ctsb/d/z*, *Osmr*) were also elevated in the DKO brains (28–30). These elevated gene expression findings suggest an inflammatory response and heightened glial reaction and were most prominently observed in *Glb1/Neu3* DKO brains compared with the other groups. Many of these genes were elevated in the *Glb1* KO brains relative to WT and *Neu3* KO brains, but to a lesser degree than in the DKO brains.

Neu3 disruption increases neurodegeneration in *Glb1* KO mouse brain

Neurodegeneration is a prominent characteristic of the GM1 gangliosidosis disease process (1, 2). To investigate the influence of NEU3 on neurodegeneration in *Glb1* KO mice, we examined the brains from 20-week-old *Glb1* KO, *Neu3* KO, *Glb1/Neu3* DKO, and WT mice using a silver-staining method to detect degenerating neuronal soma and axons (15, 31). Sagittal brain sections displayed extensive and distinct silver-grain deposition, indicative of neurodegeneration, in *Glb1/Neu3* DKO mice when compared with sections from *Glb1* KO, *Neu3* KO, and WT mice (**Fig. 4**A). Notably, the brain stem and thalamus of the DKO mice exhibited an approximately 5-fold increase in silver deposition compared with the other genotypes (Fig. 4B, C, E). In addition, a slight but statistically significant increase in silver deposition, relative to the other groups, was found in the cortex of the *Glb1/Neu3* DKO brains (Fig. 4D, E). These results demonstrate that the concurrent deletion of *Neu3* and *Glb1* significantly enhances neurodegeneration compared with the sole deletion of *Glb1* or *Neu3* in mice.

Mouse NEU3 degrades GM1 ganglioside more efficiently than human NEU3

We compared the relative amounts of GM1 ganglioside and GA1 glycolipid in an autopsy brain sample obtained from a human infantile GM1 gangliosidosis patient to the two different GM1 gangliosidosis mouse models, *Glb1* KO and *Glb1/Neu3* DKO mice, at the end stage of their disease (**Fig. 5**A). The brain sample from the human patient exhibited a higher level of GM1 ganglioside than GA1 glycolipid, as had been previously shown (19), and closely resembled the profile observed in the end-stage *Glb1/Neu3* DKO mouse brain, which also displayed a higher amount of GM1 ganglioside than GA1 glycolipid. In contrast, the end-stage *Glb1* KO mouse brain showed a higher level of GA1 glycolipid than GM1 ganglioside. These findings suggest that the sialidase-mediated conversion of GM1 ganglioside to GA1 glycolipid is more active in mice than in humans.

To further investigate the relative effectiveness of human and mouse NEU3 enzymes in degrading GM1 ganglioside to GA1 glycolipid, we transduced fibroblasts derived from an infantile GM1 gangliosidosis patient with lentivirus expressing either mouse *Neu3*, human *NEU3*, or a control vector (supplemental Fig. S2). NEU3 expression was validated by Western blotting. The fibroblasts were then loaded with BODIPY-labeled GM1 ganglioside and incubated for 72 h, after which the fluorescent BODIPY-labeled lipids were analyzed using HPTLC (Fig. 5B).

Our results revealed that the GM1 gangliosidosis fibroblasts transduced with the control vector accumulated only BODIPY-GM1 ganglioside without conversion to any other fluorescent products (Fig. 5C). However, fibroblasts overexpressing either mouse *Neu3* or human *NEU3* showed partial conversion of BODIPY-GM1 ganglioside to BODIPY-GA1 glycolipid. No additional BODIPY-labeled products were observed, indicating that the degradation process was halted after the formation of BODIPY-GA1 glycolipid. When the amount of BODIPY-GA1 glycolipid was normalized to the level of expressed NEU3 protein (Fig. 5D), mouse NEU3 was found to be approximately 2-fold more effective than human NEU3 in degrading GM1 ganglioside to GA1 glycolipid in GM1 gangliosidosis patient-derived fibroblasts (Fig. 5E).

In summary, the findings suggest that the reason for the less efficient conversion of GM1 ganglioside to GA1 glycolipid in the human GM1 gangliosidosis brain compared with the mouse GM1 gangliosidosis brain can be attributed to the decreased activity of NEU3. This difference in enzyme activity appears to be a contributing factor to the observed variations in glycosphingolipid conversion and disease severity between the two species (Fig. 5F).

DISCUSSION

Even though the *Glb1* KO mouse is a null variant, resembling the mutations that cause severe infantile type I GM1 gangliosidosis in humans, it surprisingly exhibits a disease phenotype similar to the less severe type II form (3). This disparity prompted us to investigate the potential disease-modifying role of the sialidase NEU3 as a possible explanation for the difference in disease severity between mice and humans. Our findings revealed that the absence of NEU3 exacerbated the phenotype of *Glb1* KO mice, leading to an accelerated onset of neurological symptoms, enhanced neurodegeneration, an upregulated gene expression profile indicating neuroinflammation and glial reactions, and a substantially shortened lifespan. These results strongly indicate a disease-modifying role for NEU3 in the context of GM1 gangliosidosis.

NEU3 also plays a role in modulating the severity of β-hexosaminidase A deficiency in mice. While null *HEXA* mutations lead to the extremely severe human

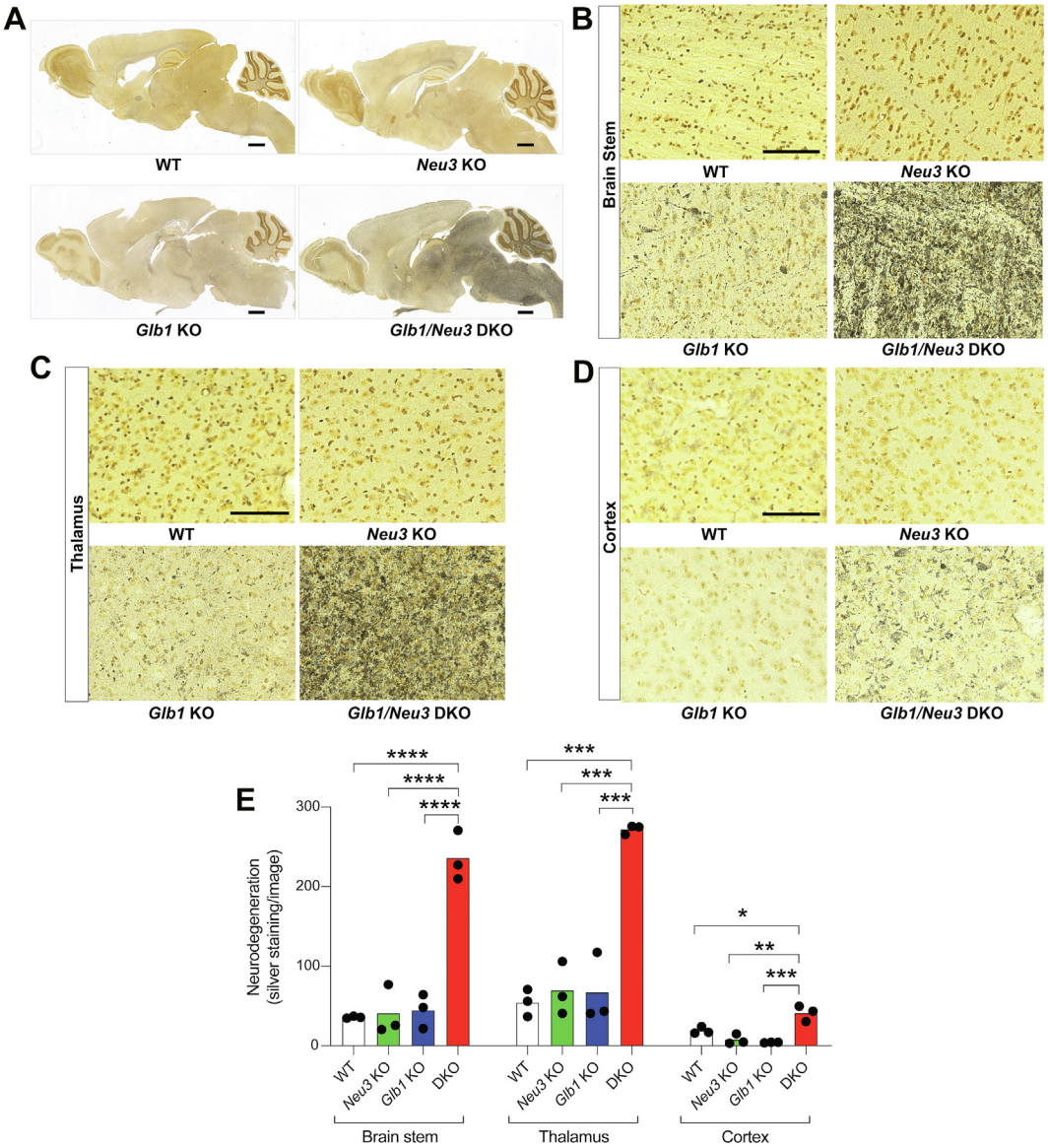

Fig. 4. *Neu3* disruption increases neurodegeneration in *Glb1* KO mouse brain. Brains from *Glb1/Neu3* DKO, *Glb1* KO, *Neu3* KO, and WT mice were harvested at 20 weeks of age. A: Brain tissue was stained with NeuroSilver to detect neurodegeneration. Representative images of sagittal sections are shown. Scale bars, 1,000 µm. B–D: Representative images of NeuroSilver-stained sections from brain stem (B), thalamus (C), and cortex (D) from WT, *Neu3* KO, *Glb1* KO, and *Glb1/Neu3* DKO mice. Scale bars, 100 µm. E: Quantification of silver-grain deposition in brain stem, thalamus, and cortex of WT, *Neu3* KO, *Glb1* KO, and *Glb1/Neu3* DKO mice calculated using Fiji/ImageJ. Data are expressed as mean intensities per brain region for each mouse. Statistical significance was determined by one-way ANOVA with Bonferroni correction, $^{*}P < 0.05$, $^{**}P < 0.01$, $^{***}P < 0.001$, and $^{****}P < 0.0001$. n = 3 brains for each genotype, three stacks per brain, 22–37 images per stack. DKO, double KO.

infantile Tay-Sachs disease, *Hexa* KO mice exhibit a much milder phenotype (32, 33). This difference can be attributed to the action of NEU3 in mice, which creates an alternate degradation pathway for GM2 ganglioside (Fig. 1A) (6), the lysosomal substrate that accumulates in Tay-Sachs disease. In *Hexa* KO mice, NEU3 cleaves GM2 ganglioside, generating GA2 glycolipid (asialo-GM2 ganglioside) as a product. GA2 glycolipid then serves as a substrate for fully intact β-hexosaminidase B, which removes the terminal β-N-acetyl-galactosamine residue. This process enables complete degradation of GM2 ganglioside in the absence of *Hexa*. In contrast, in *Glb1* KO mice, NEU3 activity results in the production of GA1 glycolipid with no other β-galactosidase activity capable of effectively removing the terminal β-galactose residue from the substrate to bypass the degradation block. As a result, the degradation pathway for GM1 ganglioside remains obstructed at GA1 glycolipid in *Glb1* KO mice.

Our findings indicate that the removal of the single sialic acid residue from GM1 ganglioside, mediated by NEU3, provides substantial protection against neurodegeneration in the context of lysosomal β-galactosidase deficiency, suggesting that GM1 ganglioside

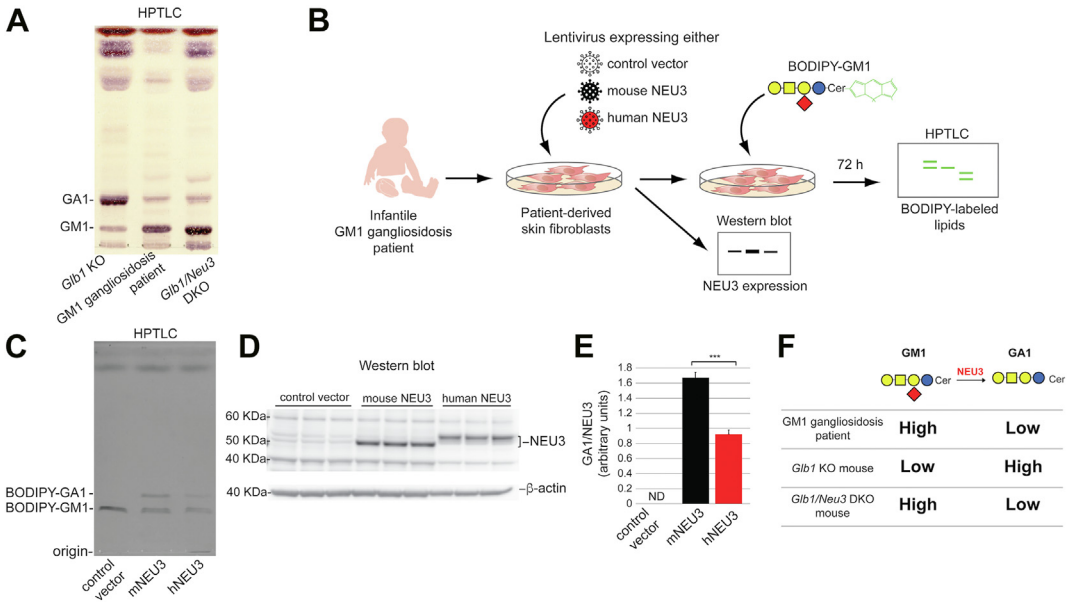

Fig. 5. Mouse NEU3 degrades GM1 ganglioside more efficiently than human NEU3. A: Gangliosides and neutral glycosphingolipids were extracted from an end-stage, 46-week-old *Glb1* KO brain, end-stage, 20-week-old *Glb1/Neu3* DKO brain, and from an autopsy cerebral-cortex sample from an infantile GM1 gangliosidosis patient. For each brain sample, an equivalent of approximately 4 mg wet-brain weight of the aqueous and organic fractions was applied to the same lane of an HPTLC plate, developed in C:M:0.25% $CaCl_2$ (60:35:5 v/v/v), and visualized using orcinol. GM1 ganglioside and GA1 glycolipid positions were identified using standards run on the same HPTLC plate. B: Schematic of experiment to determine the relative GM1 ganglioside to GA1 glycolipid degrading efficiency of mouse and human NEU3. C: HPTLC analysis of the total lipid extracts from BODIPY-GM1 ganglioside-treated patient fibroblasts expressing human *NEU3*, mouse *Neu3*, or a control vector. Total lipids were extracted after 72 h, applied to an HPTLC plate, and developed in C:M:0.25% $CaCl_2$ (60:35:5 v/v/v). Positions of BODIPY-GM1 ganglioside and BODIPY-GA1 glycolipid are shown. D: Western blot using antibody to Strep-Tag II showing the expression of NEU3 in GM1 gangliosidosis fibroblasts transduced with lentivirus (control vector, mouse *Neu3*, or human *NEU3*) (top panel) and β-actin (bottom panel). E: Relative efficiency of mouse and human NEU3 activity on GM1 ganglioside. GM1 gangliosidosis fibroblasts transduced with lentivirus (control vector, mouse *Neu3*, or human *NEU3*) were treated with BODIPY-GM1 ganglioside. After 72 h, total lipids were harvested and separated by HPTLC. Fluorescence generated by GA1 glycolipid (average of three independent fibroblast cultures) was quantified relative to the level of mouse or human NEU3 protein normalized to β-actin as determined by Western blot (average of three independent fibroblast cultures). Data are expressed as means ± SD. Statistical significance was determined by *t* test. $^{***}P < 0.001$. F: Summary of relative GM1 ganglioside to GA1 glycolipid levels in human infantile GM1 gangliosidosis brain, *Glb1* KO mouse brain and *Glb1/Neu3* DKO mouse brain. DKO, double KO; GA1, GM1 and asialo-GM1 ganglioside; HPTLC, high-performance TLC; ND, not detectable.

storage may be more neurotoxic that an equivalent amount of GA1 glycolipid storage. The accumulation of the negatively charged GM1 ganglioside in lysosomes may interfere with efficient lysosomal degradation processes of other substrates, resulting in cascades of secondarily accumulating substrates and a more rapid impairment of the lysosomal pathway (34). Accumulated GM1 ganglioside may also trigger ER stress apoptosis (35). Moreover, lysosomal accumulation of GM1 ganglioside may interfere with the function of membrane contact sites, such as those between lysosomes and mitochondria, ultimately leading to neuronal cell death and neurodegeneration (36).

NEU3 is involved in inflammatory responses in various contexts, including neuroinflammation (23, 37–40). Its presence is generally linked to heightened inflammatory reactions. However, in *Glb1* KO mice, the presence of NEU3 significantly decreased neuroinflammatory RNA profiles compared to when NEU3 was absent. These results align with the conversion of stored GM1 ganglioside to GA1 glycolipid, facilitated by NEU3 activity, resulting in lower levels of neuroinflammation. Nevertheless, due to NEU3's action on a diverse range of substrates, other modulatory effects cannot be definitively ruled out.

The *Glb1* KO mouse shares a natural history with late infantile to juvenile type II GM1 gangliosidosis patients, as opposed to the more severe infantile (type I/severe) form. This distinction is partly based on the extended lifespan of the *Glb1* KO mouse of up to about 50 weeks. The *Glb1/Neu3* DKO mouse, with its considerably shortened lifespan, rapidly progressive neurological manifestations, and a high GM1 ganglioside to GA1 glycolipid ratio as is seen in the human disease, can be considered a model for infantile GM1 gangliosidosis. This novel model is potentially a valuable tool for investigating the pathogenesis and rapid cascade of events that lead from lysosomal dysfunction to neurodegeneration in the disease and for evaluating therapeutic approaches for GM1 gangliosidosis.

Our study demonstrates that the expression of mouse NEU3 in human GM1 gangliosidosis fibroblasts leads to more efficient conversion of GM1 ganglioside to GA1 glycolipid compared with that produced by human NEU3. This finding suggests that the decreased GM1 ganglioside to GA1 glycolipid degrading activity observed in the human brain, relative to the mouse brain, may be attributed to the less efficient functioning of human NEU3. To ameliorate the disease, a potential therapeutic strategy for GM1 gangliosidosis could involve augmenting endogenous NEU3 levels to enhance GM1 ganglioside to GA1 glycolipid conversion. A similar approach has been proposed for Tay-Sachs disease, where the upregulation of NEU3 could facilitate the degradation of GM2 ganglioside, enabling its complete breakdown (6). The manipulation of endogenous NEU3 levels holds promise as a therapeutic strategy for both GM1 gangliosidosis and Tay-Sachs disease, as it may enhance the degradation of the respective gangliosides and mitigate the progression of these disorders.

Overall, our study provides new insights into the role of NEU3 in modulating the phenotype of GM1 gangliosidosis in *Glb1* KO mice. The exacerbated neurodegeneration, upregulated neuroinflammatory gene expression, and shortened lifespan observed in *Glb1/Neu3* DKO mice underscore the importance of NEU3 in ameliorating the disease course. In addition, the differential efficiency of mouse and human NEU3 sialidases in degrading GM1 highlights the species-specific differences in the underlying disease mechanisms. These findings contribute to a better understanding of GM1 gangliosidosis pathophysiology and may have implications for the development of therapeutic strategies targeting this devastating disorder.

Data availability

The RNA-seq data discussed in this publication have been deposited in NCBI's Gene Expression Omnibus69 and are accessible through GEO Series accession number GSE241844. All UVPD data files are available in massive database (massive.ucsd.edu) with accession number MSV000092791 *via* the link ftp://massive.ucsd.edu/MSV000092791/. All other data generated or analyzed during this study are included in this manuscript and supplementary information files.

Supplemental data

This article contains supplemental data.

Acknowledgments

We are grateful to the families for donating samples for this study. We thank Karolyn Garcia for assistance in the early stages of this project.

Author contributions

M. L. A., C. J. T., and R. L. P. conceptualization; M. L. A., Y. T. L., C. B., G. T., J. Y. B., E.-R. N., and V. K. J. investigation; M. L. A., Y. T. L., C. B., J. Y. B., E.-R. N., V. K. J., J. S. B., and R. L. P. formal analysis; M. L. A., V. K. J., and R. L. P. writing-original draft; M. L .A., Y. T. L., C. B., G. T., J. Y. B., E.-R. N., V. K. J., J. S. B., C. J. T., and R. L. P. writing-review and editing.

Author ORCIDs

Jenna Y. Bakir https://orcid.org/0000-0003-4314-9115
Cynthia J. Tifft https://orcid.org/0000-0002-3931-1207
Richard L. Proia https://orcid.org/0000-0003-0456-1270

Funding and additional information

This work was supported by the Intramural Research Programs of the National Institutes of Health, National Institute of Diabetes and Digestive and Kidney Diseases (R. L. P.), the National Human Genome Research Institute (C. J. T.), and National Institutes of Health R35GM139658 (J. S. B.). The content is solely the responsibility of the authors and does not necessarily represent the official views of the National Institutes of Health.

Conflict of interest

The author declares that they have no conflicts of interest with the contents of this article.

Abbreviations

DKO, double KO; GA1, GM1 ganglioside and asialo-GM1 ganglioside; HPTLC, high-performance TLC; UVPD, ultraviolet photodissociation.

Manuscript received September 13, 2023, and in revised form October 12, 2023. Published, JLR Papers in Press, October 21, 2023, https://doi.org/10.1016/j.jlr.2023.100463

REFERENCES

1. Nicoli, E. R., Annunziata, I., d'Azzo, A., Platt, F. M., Tifft, C. J., and Stepien, K. M. (2021) GM1 gangliosidosis-a mini-review. *Front. Genet.* **12**, 734878
2. Platt, F. M., d'Azzo, A., Davidson, B. L., Neufeld, E. F., and Tifft, C. J. (2018) Lysosomal storage diseases. *Nat. Rev. Dis. Primers.* **4**, 27
3. Nicoli, E. R., Huebecker, M., Han, S. T., Garcia, K., Munasinghe, J., Lizak, M., *et al.* (2023) Glb1 knockout mouse model shares natural history with type II GM1 gangliosidosis patients. *Mol. Genet. Metab.* **138**, 107508
4. Pan, X., De Aragao, C. B. P., Velasco-Martin, J. P., Priestman, D. A., Wu, H. Y., Takahashi, K., *et al.* (2017) Neuraminidases 3 and 4 regulate neuronal function by catabolizing brain gangliosides. *FASEB J.* **31**, 3467–3483
5. Miyagi, T., and Yamamoto, K. (2022) Sialidase NEU3 and its pathological significance. *Glycoconj. J.* **39**, 677–683
6. Seyrantepe, V., Demir, S. A., Timur, Z. K., Von Gerichten, J., Marsching, C., Erdemli, E., *et al.* (2018) Murine Sialidase Neu3 facilitates GM2 degradation and bypass in mouse model of Tay-Sachs disease. *Exp. Neurol.* **299**, 26–41
7. Pshezhetsky, A. V., and Ashmarina, M. (2018) Keeping it trim: roles of neuraminidases in CNS function. *Glycoconj. J.* **35**, 375–386
8. Wang, H., Yang, H., Shivalila, C. S., Dawlaty, M. M., Cheng, A. W., Zhang, F., *et al.* (2013) One-step generation of mice carrying mutations in multiple genes by CRISPR/Cas-mediated genome engineering. *Cell.* **153**, 910–918
9. Guyenet, S. J., Furrer, S. A., Damian, V. M., Baughan, T. D., La Spada, A. R., and Garden, G. A. (2010) A simple composite phenotype scoring system for evaluating mouse models of cerebellar ataxia. *J. Vis. Exp.* https://doi.org/10.3791/1787
10. Folch, J., Lees, M., and Sloane Stanley, G. H. (1957) A simple method for the isolation and purification of total lipides from animal tissues. *J. Biol. Chem.* **226**, 497–509

11. Svennerholm, L. (1963) Chromatographic separation of human brain gangliosides. *J. Neurochem.* **10**, 613–623
12. Svennerholm, L. (1956) The quantitative estimation of cerebrosides in nervous tissue. *J. Neurochem.* **1**, 42–53
13. Klein, D. R., Holden, D. D., and Brodbelt, J. S. (2016) Shotgun analysis of rough-type lipopolysaccharides using ultraviolet photodissociation mass spectrometry. *Anal. Chem.* **88**, 1044–1051
14. O'Brien, J. P., and Brodbelt, J. S. (2013) Structural characterization of gangliosides and glycolipids via ultraviolet photodissociation mass spectrometry. *Anal. Chem.* **85**, 10399–10407
15. Zhu, H., Byrnes, C., Lee, Y. T., Tuymetova, G., Duffy, H. B. D., Bakir, J. Y., *et al.* (2023) SARS-CoV-2 ORF3a expression in brain disrupts the autophagy-lysosomal pathway, impairs sphingolipid homeostasis, and drives neuropathogenesis. *FASEB J.* **37**, e22919
16. Schindelin, J., Arganda-Carreras, I., Frise, E., Kaynig, V., Longair, M., Pietzsch, T., *et al.* (2012) Fiji: an open-source platform for biological-image analysis. *Nat. Methods.* **9**, 676–682
17. Rodriguez, P. E., Maggio, B., and Cumar, F. A. (1996) Acid and enzymatic hydrolysis of the internal sialic acid residue in native and chemically modified ganglioside GM1. *J. Lipid Res.* **37**, 382–390
18. Eikelberg, D., Lehmbecker, A., Brogden, G., Tongtako, W., Hahn, K., Habierski, A., *et al.* (2020) Axonopathy and reduction of membrane resistance: key features in a new murine model of human G(M1)-Gangliosidosis. *J. Clin. Med.* **9**, 1004
19. Hahn, C. N., del Pilar Martin, M., Schroder, M., Vanier, M. T., Hara, Y., Suzuki, K., *et al.* (1997) Generalized CNS disease and massive GM1-ganglioside accumulation in mice defective in lysosomal acid beta-galactosidase. *Hum. Mol. Genet.* **6**, 205–211
20. Liu, S., Feng, Y., Huang, Y., Jiang, X., Tang, C., Tang, F., *et al.* (2021) A GM1 gangliosidosis mutant mouse model exhibits activated microglia and disturbed autophagy. *Exp. Biol. Med. (Maywood).* **246**, 1330–1341
21. Matsuda, J., Suzuki, O., Oshima, A., Ogura, A., Noguchi, Y., Yamamoto, Y., *et al.* (1997) Beta-galactosidase-deficient mouse as an animal model for GM1-gangliosidosis. *Glycoconj. J.* **14**, 729–736
22. Przybilla, M. J., Ou, L., Tabaran, A. F., Jiang, X., Sidhu, R., Kell, P. J., *et al.* (2019) Comprehensive behavioral and biochemical outcomes of novel murine models of GM1-gangliosidosis and Morquio syndrome type B. *Mol. Genet. Metab.* **126**, 139–150
23. Yamaguchi, K., Shiozaki, K., Moriya, S., Koseki, K., Wada, T., Tateno, H., *et al.* (2012) Reduced susceptibility to colitis-associated colon carcinogenesis in mice lacking plasma membrane-associated sialidase. *PLoS One.* **7**, e41132
24. Lieberman, A. P., Puertollano, R., Raben, N., Slaugenhaupt, S., Walkley, S. U., and Ballabio, A. (2012) Autophagy in lysosomal storage disorders. *Autophagy.* **8**, 719–730
25. Hammond, T. R., Dufort, C., Dissing-Olesen, L., Giera, S., Young, A., Wysoker, A., *et al.* (2019) Single-cell RNA sequencing of microglia throughout the mouse lifespan and in the injured brain reveals complex cell-state changes. *Immunity.* **50**, 253–271.e6
26. Butovsky, O., and Weiner, H. L. (2018) Microglial signatures and their role in health and disease. *Nat. Rev. Neurosci.* **19**, 622–635
27. Hernandez, V. G., Lechtenberg, K. J., Peterson, T. C., Zhu, L., Lucas, T. A., Bradshaw, K. P., *et al.* (2023) Translatome analysis reveals microglia and astrocytes to be distinct regulators of inflammation in the hyperacute and acute phases after stroke. *Glia.* **71**, 1960–1984
28. Zhao, X., Liu, S., Yang, X., Liu, Y., Liu, G., Fan, K., *et al.* (2021) Cathepsin C aggravates neuroinflammation via promoting production of CCL2 and CXCL2 in glial cells and neurons in a cryogenic brain lesion. *Neurochem. Int.* **148**, 105107
29. Nakanishi, H. (2020) Microglial cathepsin B as a key driver of inflammatory brain diseases and brain aging. *Neural Regen. Res.* **15**, 25–29
30. Allan, E. R. O., Campden, R. I., Ewanchuk, B. W., Tailor, P., Balce, D. R., McKenna, N. T., *et al.* (2017) A role for cathepsin Z in neuroinflammation provides mechanistic support for an epigenetic risk factor in multiple sclerosis. *J. Neuroinflammation.* **14**, 103
31. Gallyas, F. (1980) Chemical nature of the first products (nuclei) of the argyrophil staining. *Acta Histochem.* **67**, 145–158
32. Sango, K., Yamanaka, S., Hoffmann, A., Okuda, Y., Grinberg, A., Westphal, H., *et al.* (1995) Mouse models of Tay-Sachs and Sandhoff diseases differ in neurologic phenotype and ganglioside metabolism. *Nat. Genet.* **11**, 170–176
33. Phaneuf, D., Wakamatsu, N., Huang, J. Q., Borowski, A., Peterson, A. C., Fortunato, S. R., *et al.* (1996) Dramatically different phenotypes in mouse models of human Tay-Sachs and Sandhoff diseases. *Hum. Mol. Genet.* **5**, 1–14
34. Sandhoff, R., and Sandhoff, K. (2023) Neuronal ganglioside and glycosphingolipid (GSL) metabolism and disease: cascades of secondary metabolic errors can generate complex pathologies (in LSDs). *Adv. Neurobiol.* **29**, 333–390
35. Tessitore, A., del, P. M. M., Sano, R., Ma, Y., Mann, L., Ingrassia, A., *et al.* (2004) GM1-ganglioside-mediated activation of the unfolded protein response causes neuronal death in a neurodegenerative gangliosidosis. *Mol. Cell.* **15**, 753–766
36. Sano, R., Annunziata, I., Patterson, A., Moshiach, S., Gomero, E., Opferman, J., *et al.* (2009) GM1-ganglioside accumulation at the mitochondria-associated ER membranes links ER stress to Ca(2+)-dependent mitochondrial apoptosis. *Mol. Cell.* **36**, 500–511
37. Delaveris, C. S., Wang, C. L., Riley, N. M., Li, S., Kulkarni, R. U., and Bertozzi, C. R. (2023) Microglia mediate contact-independent neuronal pruning via secreted Neuraminidase-3 associated with extracellular vesicles. *bioRxiv.* https://doi.org/10.1101/2023.08.21.554214
38. Yang, W. H., Heithoff, D. M., Aziz, P. V., Haslund-Gourley, B., Westman, J. S., Narisawa, S., *et al.* (2018) Accelerated aging and clearance of host anti-inflammatory enzymes by discrete pathogens fuels sepsis. *Cell Host Microbe.* **24**, 500–513.e5
39. Yang, W. H., Aziz, P. V., Heithoff, D. M., Kim, Y., Ko, J. Y., Cho, J. W., *et al.* (2023) Innate mechanism of mucosal barrier erosion in the pathogenesis of acquired colitis. *iScience.* **26**, 107883
40. Howlader, M. A., Demina, E. P., Samarani, S., Guo, T., Caillon, A., Ahmad, A., *et al.* (2022) The Janus-like role of neuraminidase isoenzymes in inflammation. *FASEB J.* **36**, e22285